RSC Advances

PAPER

View Article Online
View Journal | View Issue

Cite this: *RSC Adv.*, 2023, **13**, 15747

A comparative study on the design and application of new nano benzimidazolium gemini ionic liquids for curing interfacial properties of the crude oil–water system†

Javad Saien, Mona Kharazi,* Behnaz Shokri, Morteza Torabi and Mohammad Ali Zolfigol

Gemini surface active ionic liquids (GSAILs) are considered a new prosperous class of ionic liquids and recognized as high performance materials. The present study explores the capabilities of the newly synthesized GSAILs, constructed from two benzimidazole rings attached *via* a four or a six carbon spacer, namely [C_4benzim-C_n-benzimC_4][Br_2], $n = 4$ and 6. The products were characterized with FT-IR, NMR, XRD, TGA, DTG and SEM methods and were used in curing interfacial properties of the crude oil–water system. The interfacial tension (IFT) was reduced to about 64 and 71% under critical micelle concentrations (CMCs) of 0.028 and 0.025 mol dm^{-3} at 298.2 K for $n = 4$ and 6 GSAILs, respectively. Temperature significantly assisted this effect. Both the GSAILs could transfer the wettability of the solid surface from oil-wet to water-wet. Further, stable oil/water emulsions were produced, having emulsion indices of 74.2 and 77.3% for $n = 4$ and 6 GSAILs, respectively. Compared to homologous imidazolium GSAILs, the benzimidazolium products revealed better performance in the sense of exhibiting desired effects on the investigated interfacial properties. These can be attributed to the stronger hydrophobicity of the benzimidazolium rings as well as better spreading of the molecular charges. The Frumkin isotherm could exactly reproduce the IFT data, leading to precise determination of the important adsorption and thermodynamic parameters.

Received 18th March 2023
Accepted 6th May 2023

DOI: 10.1039/d3ra01783d

rsc.li/rsc-advances

1. Introduction

Despite increasing global demand for fossil energy and chemical products, only 20 to 40% of crude oils is recovered from mature reservoirs after primary and secondary recoveries.[1] Accordingly, surfactant injection into reservoirs is an attractive process to improve capillary number, reduce the interfacial tension (IFT) between crude oil–water, generate emulsion and alter the wettability of the rocks.[2,3] The major challenges are losing performance of conventional surfactants under harsh reservoir conditions and probability of environmental damage.[4]

Surface-active ionic liquids (SAILs) with amphiphilic nature and high stability exhibit high potential to replace the conventional surfactants.[3] SAILs are well known as chemically and thermally stable, resistive under salty conditions, and non-flammable.[5,6] In view of environmental protection, contrasting to conventional surfactants, most SAILs are with low toxicity and very low vapor pressure; being considered as environmentally friendly materials with the globally harmonized system (GHS) criteria or classification labelling and packaging (CLP) regulations in addition to recyclability.[7–9] The toxicity and biodegradability of SAILs could be regulated by proper structural design.[4] In this regard, development of natural SAILs originated from fatty acids, betaine and L-carnitine ester bromides have received more attention during recent years. The natural SAILs have been prepared through various methods such as chemical synthesis and extraction from natural sources.[10]

Considering above points, studies on using SAILs in the enhanced oil recovery (EOR) has been demonstrated with great success of oil recoveries up to 90%, as well as stability and recyclability.[2,11] Cationic SAILs could be more effective since charge repulsion hinders their adsorption on the positive charge surface of carbonate rocks which constitute about 60% of the world reservoirs.[12]

Due to these advances, multicationic gemini SAILs (GSAILs) with more than one cationic and anionic part in their structure, are highly regarded.[13] In addition to imidazolium, other GSAIL families such as pyridinium, morpholinium, and pyrrolidinium have been studied. In all the cases, greater interfacial activity, lower critical micelle concentration (CMC), higher thermal

Faculty of Chemistry and Petroleum Science, Bu-Ali Sina University, Hamedan 6517838695, Iran. E-mail: kharazi.mona@yahoo.com

† Electronic supplementary information (ESI) available. See DOI: https://doi.org/10.1039/d3ra01783d

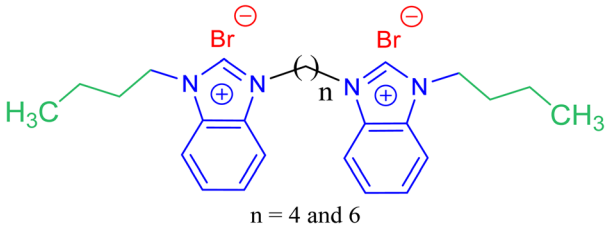

Scheme 1 The chemical structure of the used benzimidazolium based GSAILs, [C_4benzim-C_n-benzimC_4][Br_2].

resistance, easier emulsion formation and minor vapor pressure are remarkable.[14–16] Relevantly, researches have proven that extending the structure of multicationic SAILs diminishes their hazards to organisms by preventing their penetration into cell membranes.[17,18] Adding to these, nano-size particles, if relevant, significantly improve the interfacial activity and thermophysical properties of SAILs for better oil field operations.[19]

In this context, and in the continuity of our investigations in upgrading the performance of the GSAILs,[20–22] present study reports the design and synthesis of new nanostructure benzimidazolium GSAILs for curing interfacial properties of crude oil–water. Most GSAILs are based on imidazolium rings;[4] however, the target products with benzimidazole rings, a bicyclic group as fused rings of the benzene and imidazole groups, are the new endeavor of this research. The chemical structure of the target products is schematically presented in Scheme 1. Noteworthy, lipophilicity is an important parameter in the toxicity of SAILs.[23] and the longer the alkyl chains, the more possible entering SAILs into organism cells, causing membrane damage and cell death.[24,25] Thus, short alkyl chains (four carbons here) were used in design of this series of GSAILs. The products were characterized in different ways and their performance on reducing IFT, critical micelle concentration (CMC), changing surface wettability and emulsification were evaluated. Modelling of the provided data and the relevant thermodynamic parameters of Gibbs free energies of adsorption and micellization, as well as interface entropy and energy changes are sought. For deeper explanation, the results are compared with three structurally homologous imidazolium GSAILs.

2. Experimental

2.1 The used materials

The crude oil was from an oil field in south western of Iran whose major specifications and compositions are presented in Table 1. A main challenge in the SAIL applications is their cost, which inevitably limits their use in large scales. Accordingly, the price of raw materials is the main concern. Thus, low-cost and commercially available raw materials (Table 2) with high purity and reactivity were used to prepare the benzimidazolium GSAILs. The mass fraction purity and the supplier of the raw materials are itemized in Table 2. In the experiments, freshly deionized water with a conductivity of less than 0.07 μS cm^{-1} was used to prepare GSAIL solutions.

Table 1 Major specifications of the used crude oil

Specification/composition	Value
API	20.7
Saturated (wt%)	54.0
Aromatic (wt%)	22.3
Resin (wt%)	6.7
Asphalt (wt%)	7.7
Acidity number (mg KOH per g)	0.09
Sulphur content (wt%)	1.63
Salt (lbs per 1000 bbls)	4
Water content (wt%)	Nil
Density (g cm^{-3} at 20 °C)	0.915
Pour point (°F)	10
Flashpoint (°F)	70
Reid vapor pressure (psi)	12.1
Viscosity (cP at 70 °F)	55
Viscosity (cP at 100 °F)	44
Kinematic viscosity at 70 °F (cSt)	60
Loss at 200 °C (wt%)	9.3

2.2 The ionic liquids synthesis and characterization

The employed two-steps synthesis route is presented in Scheme 2. Initially, 1-butyl-1*H*-benzo[*d*]imidazole was prepared according to a previously reported procedure.[26] For this aim, benzimidazole (20 mmol, 2.36 g), 1-bromobutane (20 mmol, 2.87 g) and KOH (40 mmol, 2.24 g) were dissolved in 100 cm^3 acetonitrile and refluxed at 80 °C for 12 h. Upon completing the reaction, the solvent was evaporated and the oil was extracted with CH_2Cl_2 solvent and H_2O. After separating the organic phase, the solvent was evaporated to give the pure product of 1-butyl-1*H*-benzo[*d*]imidazole with a yield of 92%. ^{1}H NMR and ^{13}C NMR analyzes, presented in Fig. S1 and S2 in ESI,† confirmed the exact identification of the product as well as their purity. In the next step, 1,4-dibromobutane (10 mmol, 2.15 g) or 1,6-dibromohexane (10 mmol, 2.43 g), 1-butyl-1*H*-benzo[*d*]imidazole (20 mmol, 3.48 g) and 80 cm^3 of 1,4-dioxane (as solvent), were added into a 100 cm^3 round-bottomed flask. This mixture was stirred vigorously at 80 °C for 24 h under inert atmosphere until the reaction were completed. Finally, the solvent was removed at low pressure and the obtained precipitated products were washed three times with acetonitrile and dried at 60 °C to give the pure final products of [3,3′-(butane-1,4-diyl)bis(1-butyl-1*H*-benzo[*d*]imidazole-3-ium) bromide] and [3,3′-(hexane-1,6-diyl)bis(1-butyl-1*H*-benzo[*d*]imidazole-3-ium)

Table 2 Mass fraction purity of the used raw materials (all from Merck)

Material	Purity (mass fraction)
Benzimidazole	>0.98
1-Bromobutane	>0.98
1,4-Dibromobutane	>0.98
1,6-Dibromohexane	>0.98
1,4-Dioxane	≥0.99
Dichloromethane	>0.98
Acetonitrile	≥0.99.9
KOH	>0.98

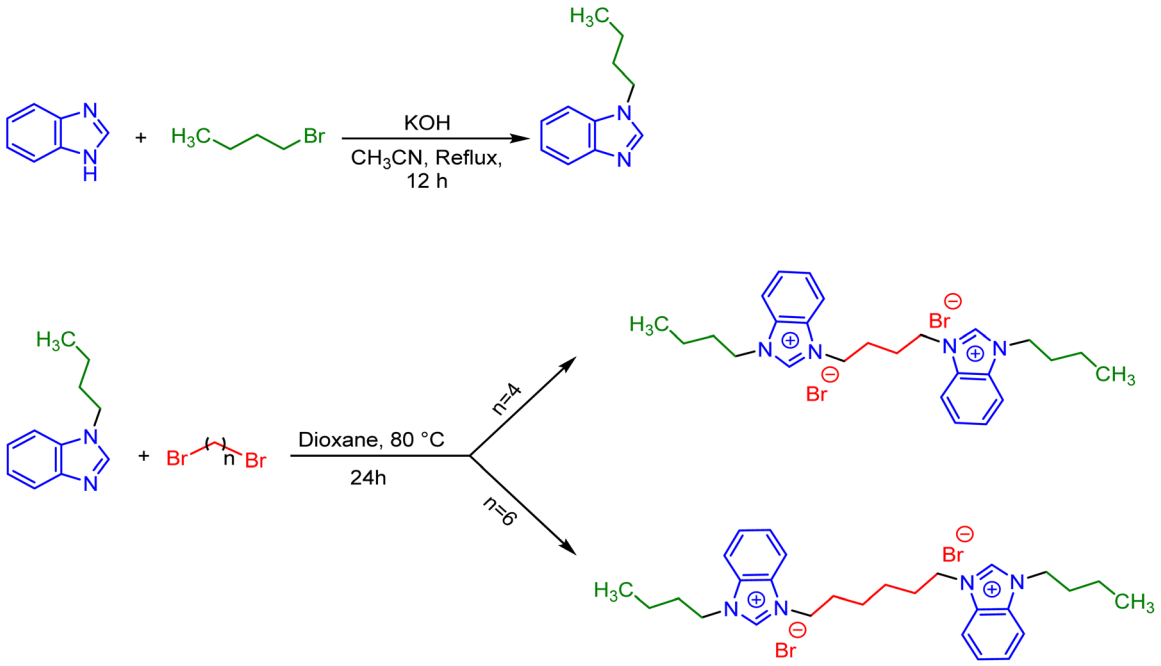

Scheme 2 The employed two-steps route for the synthesis of [C_4benzim-C_4-benzimC_4][Br_2] and [C_4benzim-C_6-benzimC_4][Br_2] gemini surface active ionic liquids.

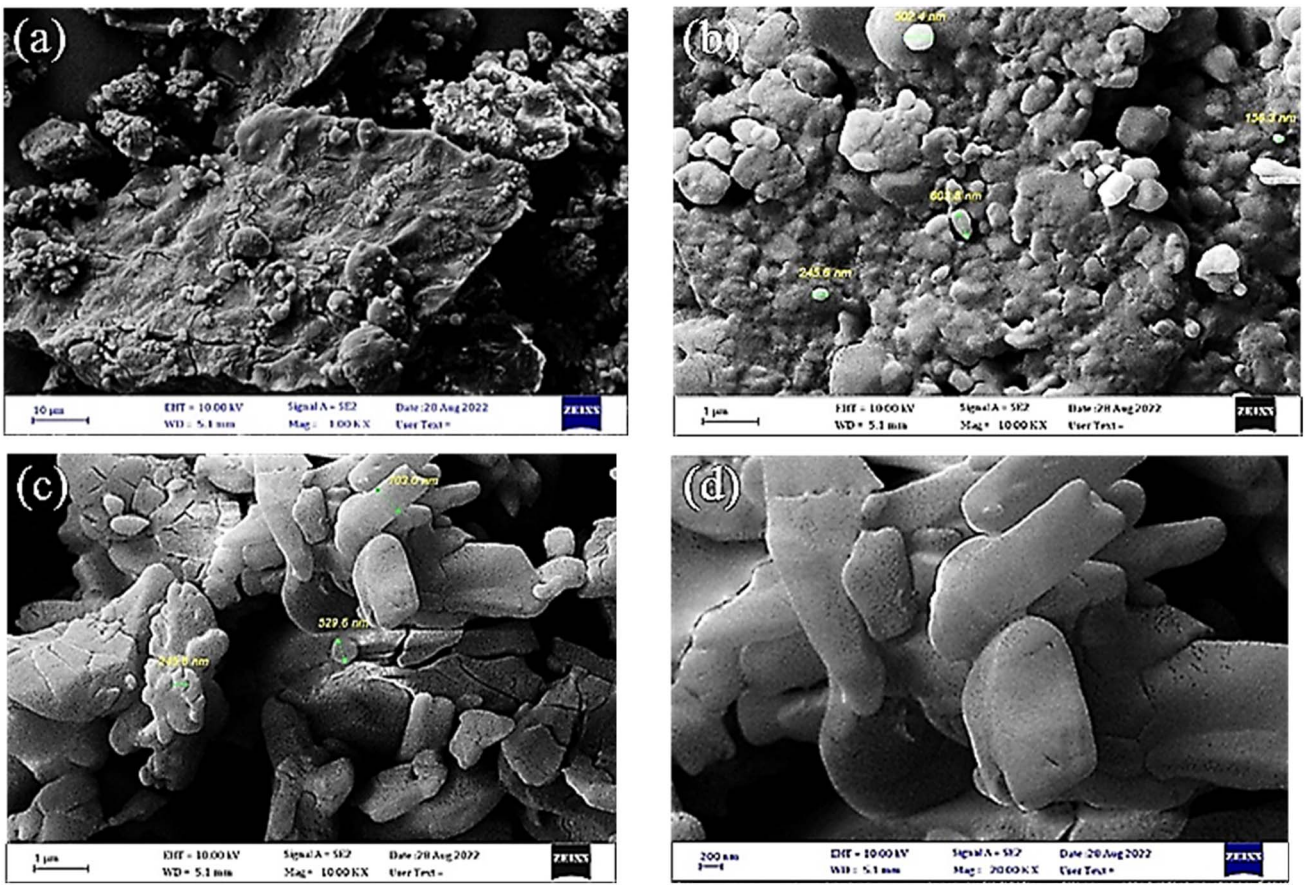

Fig. 1 The FE-SEM images for [C_4benzim-C_4-benzimC_4][Br_2] product with low (a) and high (b) magnifications and for [C_4benzim-C_6-benzimC_4][Br_2] product with low (c) and high (d) magnifications.

Table 3 The benzimidazolium GSAILs spectral data and sizes with different analysis methods

$[C_4benzim\text{-}C_4\text{-}benzimC_4][Br_2]$
FT-IR (KBr, ν, cm^{-1}): 3028, 2955, 1623, 1562, 1465, 1205, 769 ^1H NMR (250 MHz, DMSO) δ 9.99 (s, 2H), 8.09 (s, 4H), 7.66 (s, 4H), 4.58–4.48 (m, 8H), 2.01–1.87 (m, 8H), 1.30 (s, 4H), 0.89 (s, 6H) ^{13}C NMR (63 MHz, DMSO) δ 142.6, 131.5, 126.9, 46.9, 46.6, 31.3, 25.8, 19.4, 13.7 Size: XRD (10.1–36.6) nm; SEM (155 – 603) nm; DLS (2.7–10.1) nm
$[C_4benzim\text{-}C_6\text{-}benzimC_4][Br_2]$
FT-IR (KBr, ν, cm^{-1}): 3026, 2957, 1625, 1563, 1464, 1366, 1031, 768 ^1H NMR (250 MHz, DMSO) δ 10.12 (s, 2H), 8.14–8.09 (m, 4H), 7.68–7.64 (m, 4H), 4.52 (s, 8H), 1.94–1.85 (m, 8H), 1.41–1.27 (m, 8H), 0.88 (t, J = 5 Hz, 6H) ^{13}C NMR (63 MHz, DMSO) δ 142.6, 131.6, 127.0, 114.2, 66.8, 46.9, 31.0, 28.7, 25.6, 19.5, 13.8 Size: XRD (11.6–39.1) nm; SEM (103–529) nm; DLS (2.1–13.5) nm

bromide] abbreviated as $[C_4benzim\text{-}C_4\text{-}benzimC_4][Br_2]$ and $[C_4benzim\text{-}C_6\text{-}benzimC_4][Br_2]$, respectively.

The FT-IR spectra of $[C_4benzim\text{-}C_4\text{-}benzimC_4][Br_2]$ and $[C_4benzim\text{-}C_6\text{-}benzimC_4][Br_2]$ products are illustrated in Fig. S3 and S4,† respectively. According to FT-IR spectrum of $[C_4benzim\text{-}C_4\text{-}benzimC_4][Br_2]$, the diagnostic absorption band of aliphatic and aromatic C–H are shown about 3028 and 2955 cm^{-1}. The clear peak of C=N and C=C bonds are appeared at 1623 and 1562 cm^{-1}. Similarly, in FT-IR spectra of $[C_4benzim\text{-}C_6\text{-}benzimC_4][Br_2]$, aliphatic and aromatic C–H groups are illustrated about 3026 and 2957 cm^{-1}. Also, a characteristic peak at 1625 cm^{-1} and 1563 described the stretching band of C=N and C=C groups.

The ^1H NMR and ^{13}C NMR analyses assist to accurate detecting the structure of the products in addition to confirming their purity. As can be seen in ^1H-NMR spectrum of $[C_4benzim\text{-}C_4\text{-}benzimC_4][Br_2]$ (Fig. S5†), the singlet peak at chemical shift of 9.99 ppm is related to imidazolium ring proton. Other aromatic peaks are well observed at 8.09 and 7.66 ppm. The multiple peaks in the range of 4.58–4.48 ppm with the integration of eight confirmed the existence of four methylene group linked to nitrogen atoms. Two methyl groups of butyl chains are identified at 0.89 ppm and other aliphatic protons can be observed in the range of 2.01–1.30 ppm. According to ^{13}C-NMR spectrum of $[C_4benzim\text{-}C_4\text{-}benzimC_4][Br_2]$, (Fig. S6†), the number of aromatic and aliphatic carbons corresponds to the proposed structure. In addition, the structure of $[C_4benzim\text{-}C_6\text{-}benzimC_4][Br_2]$ was confirmed by ^1H-NMR and ^{13}C-NMR analysis (Fig. S7 and S8†). Notably, the peak at 40 ppm is related to deuterated DMSO (DMSO-d_6) which has been used as the solvent.

The FE-SEM images were used for investigation of the morphology and particles size of the synthetized GSAILs. In 1.00 KX magnification, the island-like morphology and the relatively irregular shapes of $[C_4benzim\text{-}C_4\text{-}benzimC_4][Br_2]$ are clearly observed in the achieved FE-SEM image (Fig. 1a). The particle size of $[C_4benzim\text{-}C_4\text{-}benzimC_4][Br_2]$ was within (155–603) nm as shown in 10.00 KX magnification (Fig. 1b). Also, $[C_4benzim\text{-}C_6\text{-}benzimC_4][Br_2]$ has irregular spherical shapes and its size is within (103–529) nm (Fig. 1c and d). Notably, previous studies have proven that the nano-sized surfactants are significantly more effective in adsorption, micelle formation, and emulsification than conventional surfactants.[27] Meanwhile, injection of nano-sized GSAILs strongly inhibits the backflow of crude oil, helps to separate oil drops from rocks, and prevents the deposition of asphaltenes.[28] Adding to these, the greater viscosity of these solutions could increase oil displacement with sweeping efficiency.[27,29]

Dynamic light scattering (DLS) analysis was also employed to determine the size of GSAIL particles and their aggregates in aqueous solutions. For this purpose, solutions of 0.01 mol dm^{-3} (less than CMC) and 0.1 mol dm^{-3} (more than CMC) were prepared and examined. The measured hydrodynamic sizes were within (2.7–10.1) nm and (2.1–13.5) nm for the C_4 and C_6

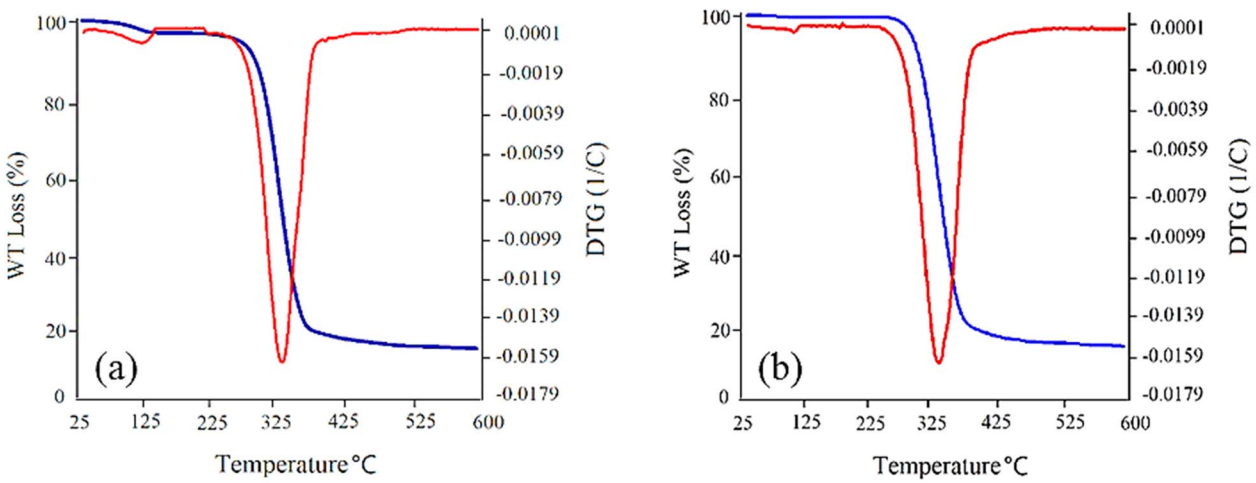

Fig. 2 TGA/DTG curves for $[C_4benzim\text{-}C_4\text{-}benzimC_4][Br_2]$ (a) and $[C_4benzim\text{-}C_6\text{-}benzimC_4][Br_2]$ (b) GSAILs.

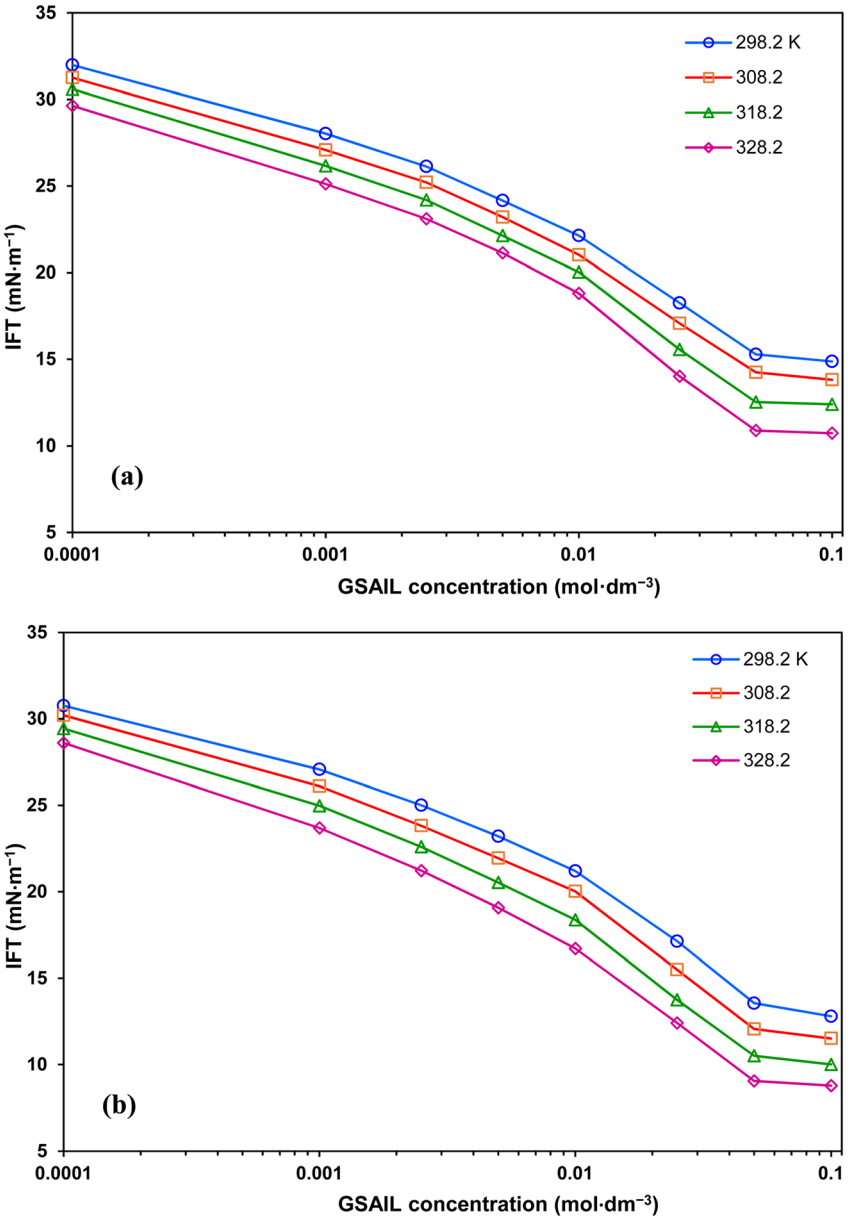

Fig. 3 IFT variations with concentration of [C_4benzim-C_4-benzimC_4][Br_2] (a), and [C_4benzim-C_6-benzimC_4][Br_2] (b) GSAILs, at different temperatures.

spacer GSAILs, respectively, and stayed within (190.1–459.4) nm and (220.2–712.3) nm for the appropriate micelle aggregates (Fig. S9 and S10†).

The XRD analysis was performed for characterization of the crystallographic structure of the GSAILs. XRD pattern of [C_4-benzim-C_4-benzimC_4][Br_2] (Fig. S11†) has the sharp diffraction lines at $2\theta = 9.55°$, 12.77°, 15.63°, 19.4°, 19.51°, 22.52°, 23.39°, 24.52° and 29.96° which confirm its rather crystal structure. Similarly, the presence of several main sharp peaks at $2\theta = 8.14$, 9.18, 11.30, 12.70, 15.20, 19.02, 22.01, 23.85, 25.49, 25.95 and 27.10 for [C_4benzim-C_6-benzimC_4][Br_2] is due to its crystal structure (Fig. S12†). To determine the crystalline sizes, the Scherrer equation, $D = K\lambda/(\beta \cos\theta)$, was used. Here, λ, β and θ denote the X-ray wavelength, the full width at the half maximum of the peak, and the Bragg diffraction angle, respectively; also K is a constant. As a result, the crystalline sizes for C_4 and C_6 spacer GSAILs were within (10.1–36.6) and (11.6–39.1) nm, respectively. Details are presented in Table S1 (ESI†). These results explains a segregated structure of the GSAILs consisting of sheets of positively charged benzimidazolium rings and bromide anions, separated by alkyl chains, as been stated by Hayes *et al.* for nanostructure ionic liquids.[30] For a better comparison, the outcomes of the mentioned analysis methods are tabulated in Table 3. It is obvious that the benzimidazolium GSAILs were correctly synthesized with nano structure both in sold state and dissolving solving in water.

Thermal stability of the synthetized GSAILs, as one important parameter in EOR, was also investigated using TGA/DTG

Table 4 Crude oil–pure water IFTs, $\gamma_{\circ}$, critical micelle concentrations, CMC, IFTs at CMC, γ_{CMC}, minimum reached IFTs, γ_{min}, and maximum reductions in IFT at different temperatures

T (K)	$\gamma_{\circ}$ (mN m^{-1})	CMC (mol dm^{-3})	γ_{CMC} (mN m^{-1})	γ_{min} (mN m^{-1})	Maximum IFT reduction (%)
			[C_4benzim-C_4-benzimC_4][Br_2]		
298.2	32.94	0.028	18.1	14.87	54.86
308.2	32.04	0.027	17.2	13.81	56.89
318.2	31.03	0.024	16.1	12.39	60.07
328.2	30.09	0.022	14.9	10.72	64.37
			[C_4benzim-C_6-benzimC_4][Br_2]		
298.2	32.94	0.025	17.0	12.80	61.14
308.2	32.04	0.024	15.5	11.51	64.08
318.2	31.03	0.023	14.5	10.01	67.74
328.2	30.09	0.020	13.6	8.78	70.82

analysis with 10 °C min^{-1} heating rate from ambient temperature to 600 °C under nitrogen atmosphere. As presented in Fig. 2a, the TGA/DTG curves of the C_4 spacer GSAIL indicate a good thermal stability and thermal decomposition at about 330 °C. In the same manner, for the C_6 spacer GSAIL a stable product is appropriate up to about 330 °C (Fig. 2b). These results are in agreement with a previous study on the thermal stability of a number of benzimidazolium Gemini ionic liquids.[31]

2.3 The main instruments and procedures

For measuring IFT and contact angle of the crude oil–aqueous phase solutions of the GSAILs, a pendant drop tensiometer (Fars EOR Technol., CA-ES10 model) equipped with digital monitoring system was used. Measurements were conducted by forming crude oil drops at the tip of a matched stainless steel needle which was immersed in the continuous water phase. The details of the setup and the method have been described in our previous studies.[22,32] Accordingly, the IFT(γ) was determined by analyzing the shape of a formed drop in relation to the balance of buoyancy and interfacial forces in connection with an automatic image processing system based on the following equation:[33]

$$\gamma = \frac{\Delta\rho g D^2}{H} \quad (1)$$

where $\Delta\rho$ represents the difference between crude oil and an aqueous solution densities, g indicates the gravitational acceleration constant, D is the equatorial diameter, and also H is the shape parameter reported in the literature.[34]

Using this method, an IFT of 31.8 mN m^{-1} was measured for pure crude oil–water system at 298.2 K. To ensure the accuracy, the IFT of pure water–air was also measured at 298.2 K (here as surface tension). The corresponding value of 71.9 mN m^{-1} was too close to 72.0 mN m^{-1} reported in the literature.[35] To confirm consistency, each measurement was repeated at least two times. Table S2† shows the details of the obtained values.

Before starting the experiments, different aqueous solutions of GSAILs were prepared in the concentration range of (1.0 × 10^{-4} to 0.1) mol dm^{-3}. To this end, GSAILs were weighed using a 0.0001 g digital balance (Ohaus Adventurer Pro, AV 264). It is important to mention that the used GSAILs solutions could be reused several times (at least 10 times) with no significant change in their function. All measurements were carried out under ambient pressure and four temperatures, within (298.2–328.2) K, adjusted with the aid of a well-tuned electric heater and a sensor (0.1 K uncertainty). The density of a solution, at specified temperatures, was obtained by means of a U-tube oscillating densitometer (Anton Paar, DMA 4500, uncertainty 1.0 × 10^{-4} g cm^{-3}), with capability of automatic viscosity correction. The data achieved for all solutions are listed in Table S2.† Also, at each temperature, CMCs were determined from the intersection of the upper and lower tangent lines of the breakpoint region in the IFT *versus* the GSAIL concentration graphs.

To measure the contact angles, the quartz plate was first immersed in the crude oil for 14 to 18 hours for aging to approximate the real reservoir conditions. Subsequently, in each measurement, the crude oil was injected *via* a needle into the aqueous phase to release a drop to adhere to the quartz surface located at the top of the cell.[36] After at least one hour, the image of the drop was recorded. The contact angles were then determined by geometry analyzing of the hemisphere crude oil drop surrounded by a GSAIL solutions. An average contact angle for the left and right sides of the drop was automatically detected. All measurements were carried out at least twice to establish consistent results.

To evaluate the capability of creating stable emulsions, equal volumes (2 cm^3) of the crude oil and the aqueous GSAIL solutions with a typical concentration of 0.01 mol dm^{-3} (corresponding to an intermediate IFT) were transferred to the glass vials and sonicated in a 40 kHz, 305 W ultrasound bath (SONICA 2400ETH S3) for 30 min. After resting for one day and one week at 298.2 K, the resultant emulsion indices were obtained from $V_e/V_t \times 100$ equation[37] in which, V_e and V_t represent the formed emulsion and the total sample volumes in the vial, respectively. In the next step, emulsion microscopic images were prepared to observe the dispersion of droplets on the glass lames using a BX-60 Olympus loupe microscope (45× magnification).

3. Results and discussion

3.1 IFT variations

The variations of the system IFT against the concentration of [C_4benzim-C_4-benzimC_4][Br_2] and [C_4benzim-C_6-benzimC_4][Br_2] GSAILs are presented in Fig. 3. Evidently, presence of GSAILs, up to CMC, brings about drastic decrease in the system IFT to 10.7 and 8.8 mN m^{-1} (maximum reductions of 64.4 and 70.8%) respectively with $n = 4$ and 6 GSAILs at a typical temperature of 328.2 K. Achieving low IFTs is required in EOR process, as it increases the capillary number in the oil reservoirs.[38,39] An attractive economic case is achieving reductions more than 50% in IFT at concentrations below 0.03 mol dm^{-3}, which is significantly cost-effective.[40] Moreover, results indicate low CMC values of less than 0.028 mol dm^{-3}. At a typical temperature of 298.2 K, CMCs are 0.028 and 0.025 mol dm^{-3} for the GSAILs with $n = 4$ and 6, respectively. Upon reaching a CMC, the surfactant molecules are forced to self-assemble spontaneously forming micelle in the bulk. It can be seen in Fig. 3 that after this concentration, the IFT remains almost constant. For better explanation, all obtained values for different temperatures are listed in Table 4.

The strong capability in reducing IFT is due to the amphiphilic nature of the benzimidazolium GSAILs, giving high tendency to migrate toward the interface. Under this condition, the hydrophobic segments in the GSAIL molecules, containing the side chains and the aromatic rings locate in the crude oil, while the positively charged hydrophilic nitrogen-containing rings tend to be in the aqueous phase (Fig. 4). Thus, adsorbed species find the lowest free energy and the phase intermolecular forces are minimum leading to the maximum reduction in IFT. Hence, the spacer and the aromatic benzimidazolium rings in the GSAILs, by spreading molecular charge, reduce electrostatic repulsion and give close packing at the interface.[3]

A comparison on results reveals that the longer spacer ($n = 6$) GSAIL is profound with a 6.5% greater IFT reduction at a typical temperature of 298.2 K. This can be attributed to the greater hydrophobicity of the more carbon atom spacer. Also, the wider configuration of the longer spacer GSAIL at the interface weakens more the intermolecular forces.[41] Regarding CMC, the long spacer GSAIL shows about 10% lower CMC than the short spacer one at different temperatures. Indeed, the greater hydrophobic parts in the larger spacer GSAIL forces molecules to self-assemble at lower concentrations.

In EOR, surfactants must withstand the dominant high temperatures in reservoirs for long times. Accordingly, Fig. 5 shows that temperature gives additional reductions in IFT. The highest decrease was about 38.7 and 45.8% for the short and the long spacer GSAILs, respectively, compared to that at 298.2 K, under a typical concentration of 0.1 mol dm^{-3}. Thus, consistent to the TGA/DTG analysis that confirmed the thermal stability of benzimidazolium GSAILs; temperature helps to improve interfacial activity in contrast to conventional surfactants that lose their activity at high temperatures.

Further, destruction of water accumulations around the GSAIL particles decreases the CMCs (Table 4). Under these conditions, the molecules move more freely in the bulk and the hydrophobic parts accumulate easily at low concentrations.[19] Therefore, in terms of CMC, a higher temperature is favorable. It is worth noting that a lower CMC is desired for EOR because it is beneficial for the transport of oil droplets with micelles in the "surfactant flooding" process.[4]

3.2 Wettability alteration

Wettability represents the interaction between crude oil and brine solution in contact with the rock surface of the reservoir, known as a critical parameter affecting the original oil in place (OOIP). As the wettability changes from oil-wet to water-wet, the residual oil will separate easily from the surface of the reservoir rocks. This increases the mobility of the crude oil leading to a significant increase in EOR. Wettability can be quantified with

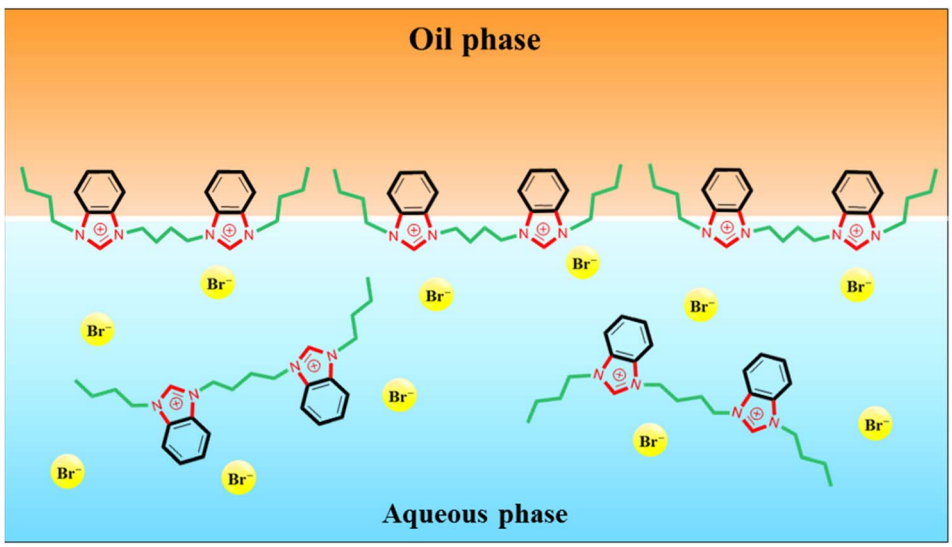

Fig. 4 Schematic of the [C_4benzim-C_4-benzimC_4][Br_2] configuration in the crude oil–water system.

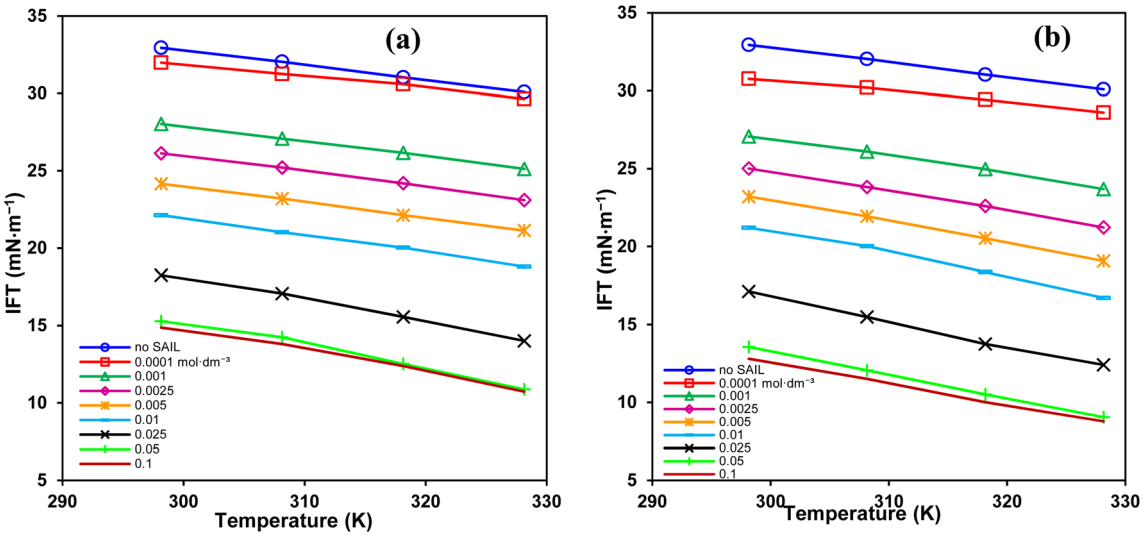

Fig. 5 IFT variation *vs.* temperature for different concentrations of [C_4benzim-C_4-benzimC_4][Br_2] (a), and [C_4benzim-C_6-benzimC_4][Br_2] (b) GSAILs.

the contact angle of drops with the surface. In a crude oil–water–rock contact, reservoir surfaces are classified as hydrophilic (water-wet) with the contact angles between (0–80°), moderate (intermediate-wet) with the contact angles between (80–100°), and hydrophobic (oil-wet) with the contact angles between (100–180°).[42] Noteworthy, for an oil drop, formed in the aqueous phase, the external contact angles are considered.

The appeared shapes of the attached drops, surrounded by each of the GSAIL solutions on the solid surface, are illustrated in Fig. 6. The corresponding contact angles of crude oil drops measured at the 298.2 K are also presented in Fig. 7. As it is possible to see, the contact angle of 161° in crude oil-pure water is highly reduced to 23° and 12°, with a 0.05 mol dm^{-3} of the short and the long spacer GSAILs, respectively. Thus, in addition to the previously mentioned improvements, the benzimidazolium GSAILs by accumulating on both the oil drops and the solid surface, can alter the oil-wet surface to water-wet.

3.3 Emulsifying capability

In the process of crude oil recovery, transferring surfactants to the low permeable zones and dissolving crude oils by forming

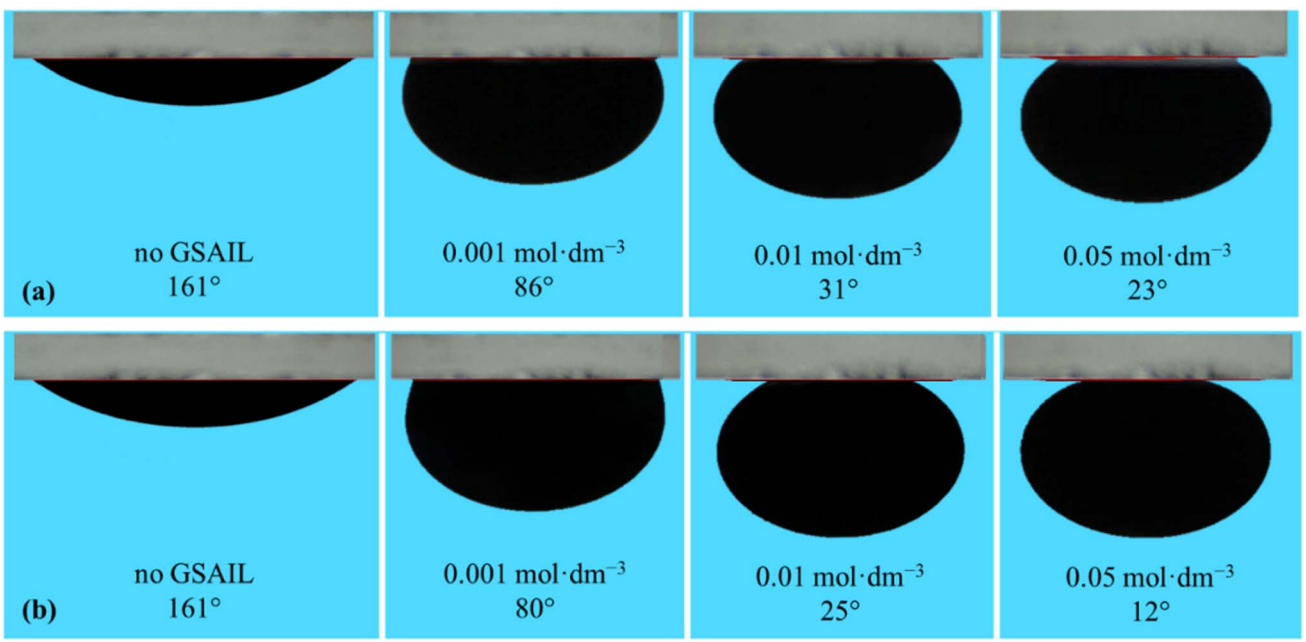

Fig. 6 The shapes of the crude oil drops surrounded with different aqueous solutions of [C_4benzim-C_4-benzimC_4][Br_2] (a), and [C_4benzim-C_6-benzimC_4][Br_2] (b) GSAILs on the quartz surface at 298.2 K.

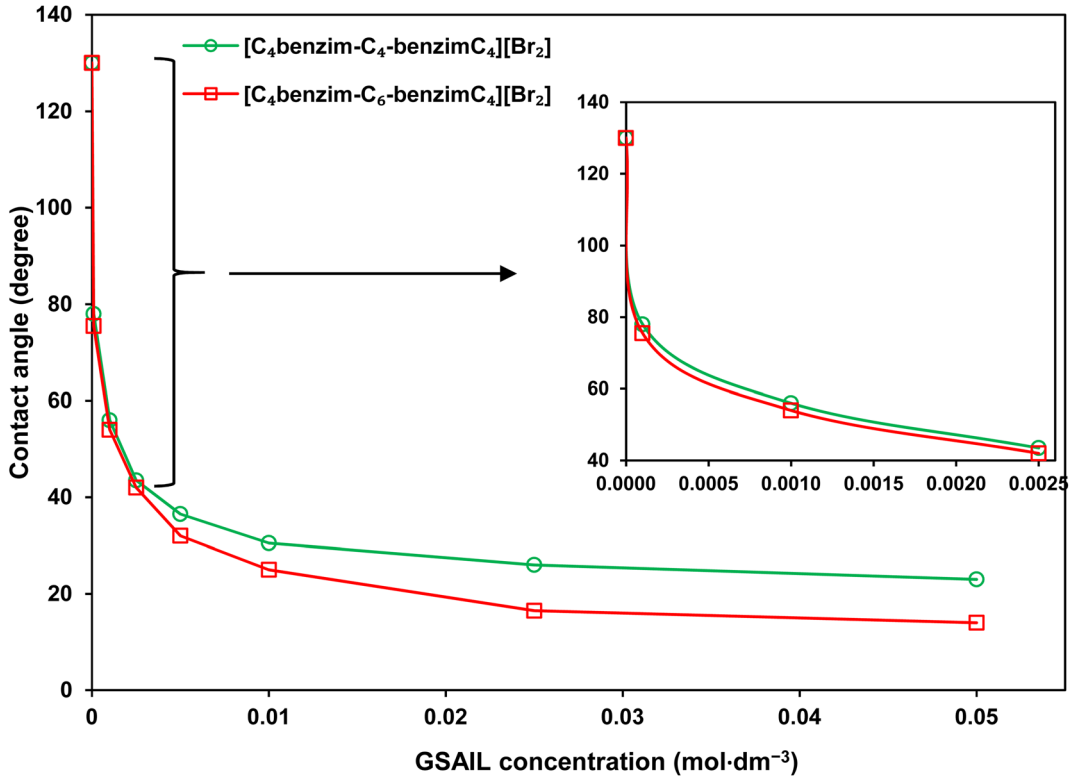

Fig. 7 The contact angles of crude oil drops surrounded with the GSAIL aqueous solutions on the quartz surface at 298.2 K.

stable oil–in–water (O/W) or multiple emulsions is vital. Noteworthy, formation of emulsions diminishes adsorption of crude oil on the surface of reservoir rocks and consequently smooths the movement of the residual crude oil.[43] Besides, emulsion facilitates the flow of injection fluids in non-swept areas, blocks permeable pathways to inhibit the crude oil backflow, raises the viscosity of the displacement medium, and greatly improves the mobility as well as the sweeping efficiency.[44,45] Of course, a low IFT is essential for the formation of a stable emulsion.[46] As was described above, the high performance of the benzimidazolium GSAILs in reducing IFT was explored. Noteworthy, creating stable emulsions with conventional surfactants regularly requires co-surfactants that are volatile and cause environmental hazards.[4] However, due to high interfacial activity, GSAILs could form stable emulsions without using a co-surfactant.[47,48]

The images of the crude oil–water (no GSAIL) emulsions and with typical 0.01 mol dm^{-3} of the GSAILs, along with their microscopic images are presented in Fig. 8. As is clear, no emulsion was formed with no GSAIL; however GSAIL solutions could bring about emulsion indices as high as high as 74.2 and 70.8% with the C_4 spacer and 77.3 and 74.6% with the C_6 spacer GSAILs, respectively, after one day and one week. These confirm that the benzimidazolium GSAILs are proper candidates for EOR by emulsification method. Also, the emulsions were monitored after two months and their stability was proved. In the same manner, it is clear from microscopic images that the presence of GSAILs causes almost uniform O/W dispersions. This is a consequence of the strong amphiphilic nature of the benzimidazolium GSAILs, leading to directional adsorption around the interface of crude oil droplets and formation of hydrophilic protective films, playing a prominent role in the dispersion.[49] As well, reduction of IFT promotes the formation of the emulsions. Meanwhile, the positive charged nitrogen atoms in the benzimidazolium rings create protective layers around the droplets, repel them electrostatically and give better separation and stabilization. In other words, GSAILs with large and bulky benzimidazolium head groups sterically hinder droplets coalescence.[3]

4. Theoretical consideration

The famous Frumkin adsorption isotherm acceptably covered the experimental IFT data at concentrations below CMC under the various investigated temperatures. This isotherm takes into account the non-ideal interactions (attraction or repulsion) among adsorbed particles at the interfaces.[50] Considering the two positively charged benzimidazole rings that establish strong interfacial interaction between GSAIL adsorbates, the use of this isotherm is consistent. The equation of state and the isotherm are as:[51]

$$\Pi = -2RTT_{m,F}[\ln(1-\theta) + \beta\theta^2] \quad (2)$$

$$b_F f_{\pm}\left[C\left(C + C_{electrolyte}\right)\right]^{1/2} = \frac{\theta}{1-\theta}\exp(-n\beta\theta) \quad (3)$$

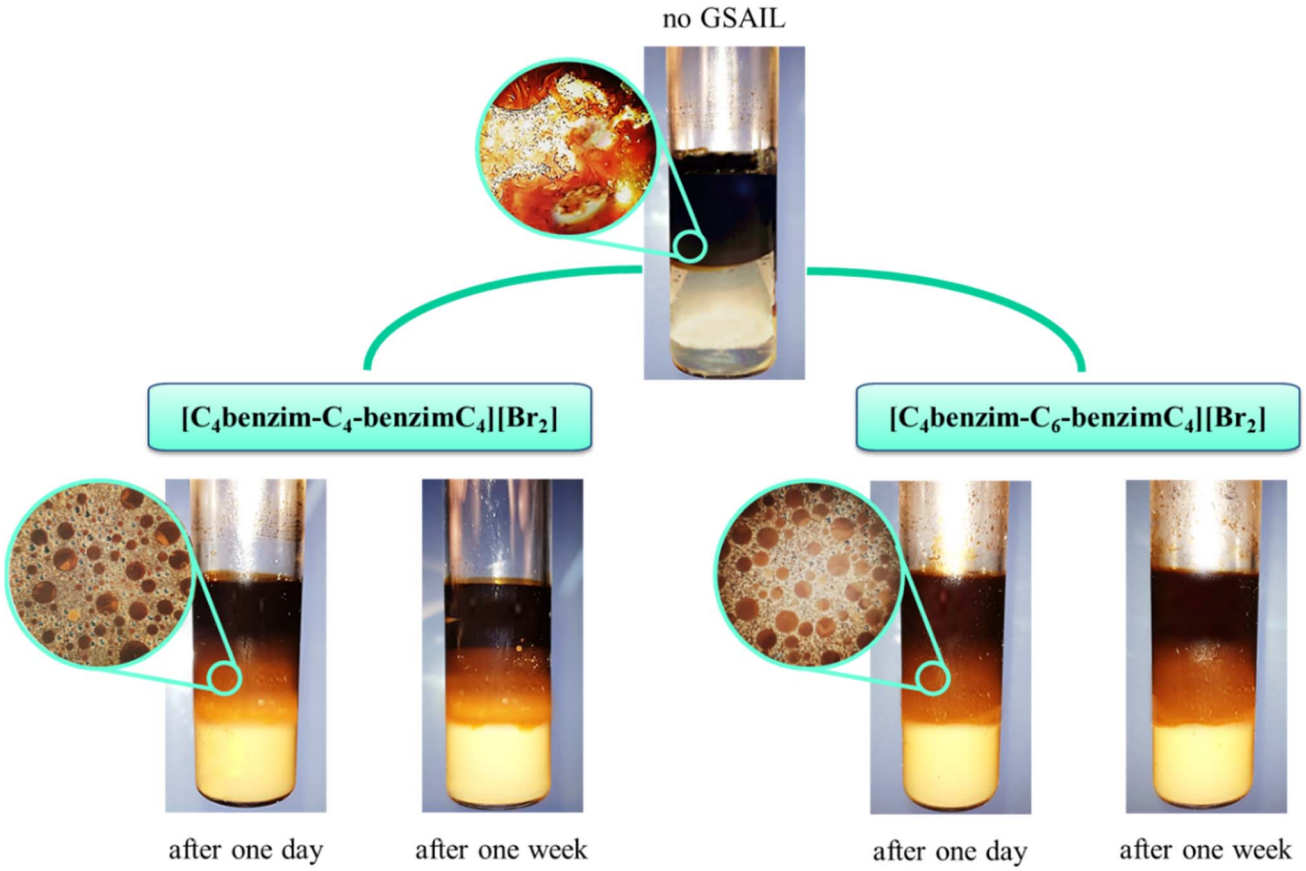

Fig. 8 The crude oil–water emulsions and the microscopic images (45× magnification) with no GSAILs and with 0.01 mol dm^{-3} of the GSAILs after one day and after one week.

In these equations, $\Pi = \gamma_\circ - \gamma$, known as interfacial pressure, represents the difference between the pure system IFT, $\gamma_\circ$, and the achieved value, γ. Besides, $\theta = \Gamma/\Gamma_{m,F}$ shows the interface coverage. Other parameters are described according to the Gibbs dividing interface theory on which the Frumkin isotherm is based,[51] including the maximum interface excess concentration in Frumkin model, $\Gamma_{m,F}$, the Frumkin adsorption constant, b_F, the van der Waals molecular interaction parameter, β, and the activity coefficient of ions, $f_\pm$. The correctness of fittings of the experimental data with the Frumkin isotherm is proven by achieving the minimum value of the objective function (OF) as:[52]

$$\mathrm{OF} = \sum_{i=1}^{m} \frac{\Delta C_i}{C_{\mathrm{exp},i}} \frac{\Delta \Pi_i}{\Pi_m - \Pi_1} \quad (4)$$

where $\Delta C_i = |C_{\mathrm{exp},i} - C_{\mathrm{cal},i}|$ and $\Delta \Pi_i = (\Pi_{\mathrm{exp},i+1} - \Pi_{\mathrm{exp},i-1})/2$, respectively, represent the difference of experimental and calculated concentrations and interfacial pressure values of the ith data point. Besides, $\Pi_m = \gamma_\circ - \gamma_m$ is the maximum interfacial pressure compared to the γ_m of the last IFT in a series

Table 5 The maximum interface excess concentration, $\Gamma_{m,F}$, the Frumkin adsorption constant, b_F, the interaction parameter, β, the minimum occupied interface area by each molecule, A_m, and the objective function, OF, relevant to the GSAILs at different temperatures

T (K)	$\Gamma_{m,F} \times 10^6$ (mol m^{-2})	b_F (dm^3 mol^{-1})	β	$A_m \times 10^{36}$ (m^2)	OF
		[C$_4$benzim-C$_4$-benzimC$_4$][Br$_2$]			
298.2	1.67	212.4	−4.0	6.98	2.17×10^{-2}
308.2	2.08	166.1	−4.8	5.59	2.27×10^{-2}
318.2	2.44	148.7	−5.4	4.77	3.56×10^{-2}
328.2	2.82	135.3	−6.2	4.13	4.15×10^{-2}
		[C$_4$benzim-C$_6$-benzimC$_4$][Br$_2$]			
298.2	1.69	269.2	−3.9	6.87	3.54×10^{-2}
308.2	2.13	222.5	−4.7	5.47	4.32×10^{-2}
318.2	2.50	211.6	−5.3	4.66	3.58×10^{-2}
328.2	2.86	207.4	−6.1	4.07	2.07×10^{-2}

Table 6 Gibbs free energy of adsorption, $\Delta G°_{ads}$, Gibbs free energy of micellization, $\Delta G°_{mic}$, and the molar concentration of water, ρ', of the GSAILs at different temperatures

T (K)	$\Delta G°_{ads}$ (kJ mol^{-1})	$\Delta G°_{mic}$ (kJ mol^{-1})	$\rho' \times 10^3$ (mol cm^{-3})
	[C_4benzim-C_4-benzimC_4][Br_2]		
298.2	−42.99	−9.46	55.38
308.2	−43.17	−10.02	55.20
318.2	−43.97	−10.62	54.89
328.2	−44.78	−11.28	54.47
	[C_4benzim-C_6-benzimC_4][Br_2]		
298.2	−44.18	−9.82	55.39
308.2	−44.66	−10.43	55.21
318.2	−45.84	−11.10	54.89
328.2	−47.11	−11.95	54.48

which includes m data points. The IsoFit software was employed for performing calculations. As presented in Fig. S13 and S14,† the adsorption isotherm of Frumkin fits the data well. Consequently, the achieved fitting parameters and the OF values at each temperature are listed in Table 5.

Within the temperature range, the OF values were in the range of (0.021–0.043) for the GSAILs confirming good fittings. It is clearly seen that $\Gamma_{m,F}$ of the long spacer GSAIL ($n = 6$) is higher than the short one ($n = 4$), which is consistent with the above mentioned results and can be attributed to the greater hydrophobicity and adsorption tendency as was described in Section 3.1. The negative values of the molecular interaction parameter, β, confirm the existence of electrostatic repulsion among the adsorbed GSAILs with positively charged head groups. However, the absolute value of β decreases with increasing spacer length, since a longer spacer and the more spread of the molecular charge, reduce the electrostatic repulsion. In the same manner, the Frumkin adsorption constant, b_F, increases with the length of spacer, giving a greater hydrophobicity and leading to higher adsorption tendency. Relevantly, the minimum occupied interface area by each adsorbed molecule, A_m, is as:

$$A_m = \frac{1}{\Gamma_{m,F} N_{Av}} \quad (5)$$

where N_{Av} is the Avogadro's number. As expected, the compact orientation of the long spacer [C_4benzim-C_6-benzimC_4][Br_2] molecules at the interface gives a lower occupied area by each molecule compared to the short spacer one.

In view of the temperature effect, $\Gamma_{m,F}$ increases with temperatures. This can be ascribed to improving mobility of the GSAIL particles and also dehydration of the hydrophilic parts. Accordingly, temperature rises the interfacial concentration and the compact orientation of particles in the adsorption layer, which decreases reasonably the occupied area by each molecule, A_m. In the same manner, a tighter interface arrangement of adsorbed particles at high temperatures reflects larger electrostatic repulsion, β. In contrast, the Frumkin adsorption constant, b_F, is diminished with temperature, which can be due to the fact that temperature increases the electrostatic repulsion, lowering the adsorption tendency.

The thermodynamic parameters of $\Delta G°_{ads}$ and $\Delta G°_{mic}$, related to adsorption and micellization Gibbs free energies, reflecting the adsorption and aggregation tendencies, are determined by:[52,53]

$$\Delta G°_{ads} = -2RT \ln\left(\frac{b_F \rho'}{2}\right) \quad (6)$$

$$\Delta G°_{mic} = RT \ln CMC \quad (7)$$

while $\rho' = \rho/18$ is the molar concentration of water. As listed in Table 6, negative values of Gibbs free energies approve the GSAILs adsorption at crude oil–water interface as well as the micellization were spontaneous. However, superior hydrophobicity with a higher spread of the molecular charge provides greater forces for the C_6 spacer GSAIL. At higher temperatures, thermal mobility increases the total free energy of adsorption. As well, dehydration of the hydrophilic parts of the GSAILs in the bulk, increases the aggregation tendency with temperature. As another point, the absolute values of $\Delta G°_{ads}$ are meaningfully greater than $\Delta G°_{mic}$, implying that the GSAILs prefer to be adsorbed rather than creating aggregates in the bulk.

As a final point, the interface entropy change, ΔS, as well as the energy change, ΔU, were obtained from:[54]

$$\Delta S = -\left(\frac{\partial \gamma}{\partial T}\right)_{p,C} \quad (8)$$

$$\Delta U = \gamma + T\Delta S \quad (9)$$

Variations of ΔS and ΔU with temperature for the GSAILs are presented in Fig. S15 to S18,† respectively. The specific changes of ΔS with temperature are due to the competing phenomena of improved particles agitation and dehydration of GSAIL molecules at the interface.[55] The former causes an increase in the entropy and the latter makes a strong van der Waals attraction between the GSAIL molecules, which decreases the entropy.[56] Because of dependency on ΔS, a similar variation trend is observed for ΔU.

5. Comparative study

In order to deeper investigate the performance of the benzimidazolium GSAILs, a comparison was made with three homologous imidazolium GSAILs consisting of two

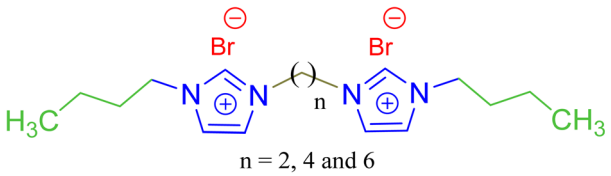

n = 2, 4 and 6

Scheme 3 The chemical structure of the homologous imidazolium based GSAILs: [C_4im-C_n-imC_4][Br_2].

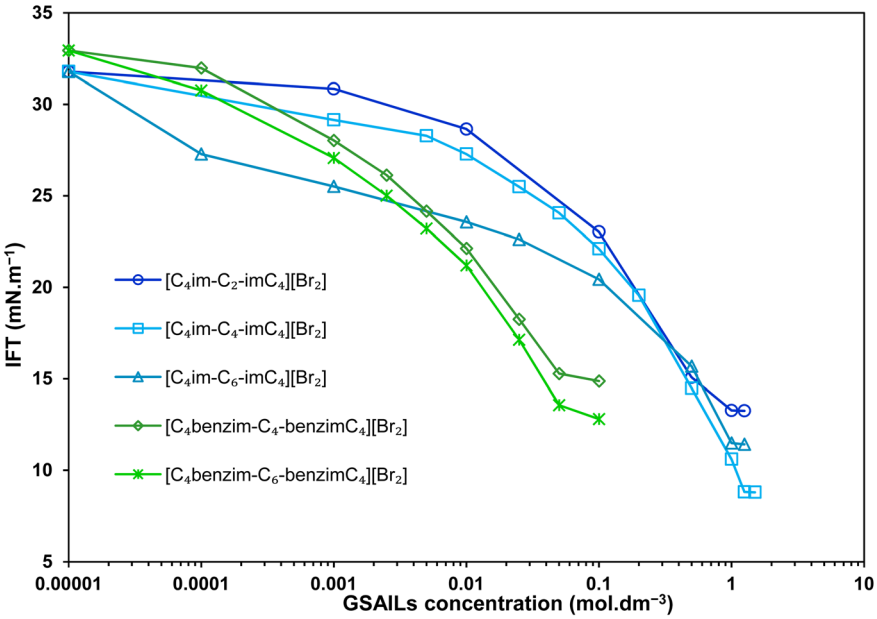

Fig. 9 IFT variations *vs.* concentration with the benzimidazolium GSAILs compared to the homologous imidazolium GSAILs at 298.2 K.

imidazolium rings and alkyl chains of four carbons, attached by different spacers, as $[C_4im\text{-}C_n\text{-}imC_4][Br_2]$ $n = 2$, 4 and 6. The molecular structure of these imidazolium GSAILs are presented in Scheme 3.

The variation of crude oil–water IFT with concentration at a typical temperature of 298.2 K is shown in Fig. 9. To achieve a typical IFT of 16 mN m^{-1}, for instance, the required amounts benzimidazolium GSAILs are only about 0.05 and 0.03 mol dm^{-3}, for the C_4 and C_6 spacer GSAILs, respectively; however, more than 0.4 to 0.6 mol dm^{-3} of the imidazolium GSAILs are needed. It could be concluded that the hydrophobic aromatic rings provide higher interfacial activity for the benzimidazolium GSAILs. The benzimidazole rings also better spread the electrostatic repulsion between positive charge head groups and provide easier adsorption. This is also verified by the lower van der Waals molecular interaction, β, values (Table 7). Further, comparison between the $\Gamma_{m,F}$ values confirms the above results. However, the higher hydrophobicity of the rings reduces the water solubility of benzimidazolium GSAILs, which makes them unable to achieve an ultimate low IFT by the imidazolium GSAILs.

Regarding CMC, much lower CMCs were obtained by the benzimidazolium GSAILs, which offers an average 96.6 to 97.4% lower values compared to the imidazolium GSAILs (Fig. 10). As

Table 7 The maximum interface excess concentration, $\Gamma_{m,F}$, the minimum interface area occupied by each molecule, b_F, the Frumkin adsorption equilibrium constant, β, the molecular interaction parameter, $f_{\pm}$, the Gibbs free energy of adsorption, $\Delta G°_{ads}$, and the Gibbs free energy of micellization, $\Delta G°_{mic}$, of imidazolium GSAILs at different temperatures

T (K)	$\Gamma_{m,F} \times 10^6$ (mol m^{-2})	$A_m \times 10^{36}$ (m^2)	b_F (dm^3 mol^{-1})	β	$\Delta G°_{ads}$ (kJ mol^{-1})	$\Delta G°_{mic}$ (kJ mol^{-1})
			$[C_4im\text{-}C_2\text{-}imC_4][Br_2]$			
298.2	1.28	9.08	109.5	−1.5	−39.73	−0.49
308.2	1.80	6.48	421.6	−1.9	−36.15	−0.51
318.2	2.32	5.02	259.9	−2.5	−34.74	−0.53
328.2	3.38	3.45	364.8	−6.1	−37.64	−0.56
			$[C_4im\text{-}C_4\text{-}imC_4][Br_2]$			
298.2	2.78	4.19	476.7	−4.1	−47.02	−0.003
308.2	3.70	3.14	159.7	−5.0	−42.98	−0.01
318.2	5.00	2.33	83.1	−6.8	−40.88	−0.03
328.2	6.25	1.86	92.8	−9.9	−42.73	−0.06
			$[C_4im\text{-}C_6\text{-}imC_4][Br_2]$			
298.2	1.39	8.38	991.0	−6.1	−47.02	−0.25
308.2	1.43	8.15	807.9	−7.7	−42.98	−0.27
318.2	1.54	7.57	684.8	−8.5	−40.88	−0.30
328.2	1.83	6.34	702.1	−10.2	−42.73	−0.34

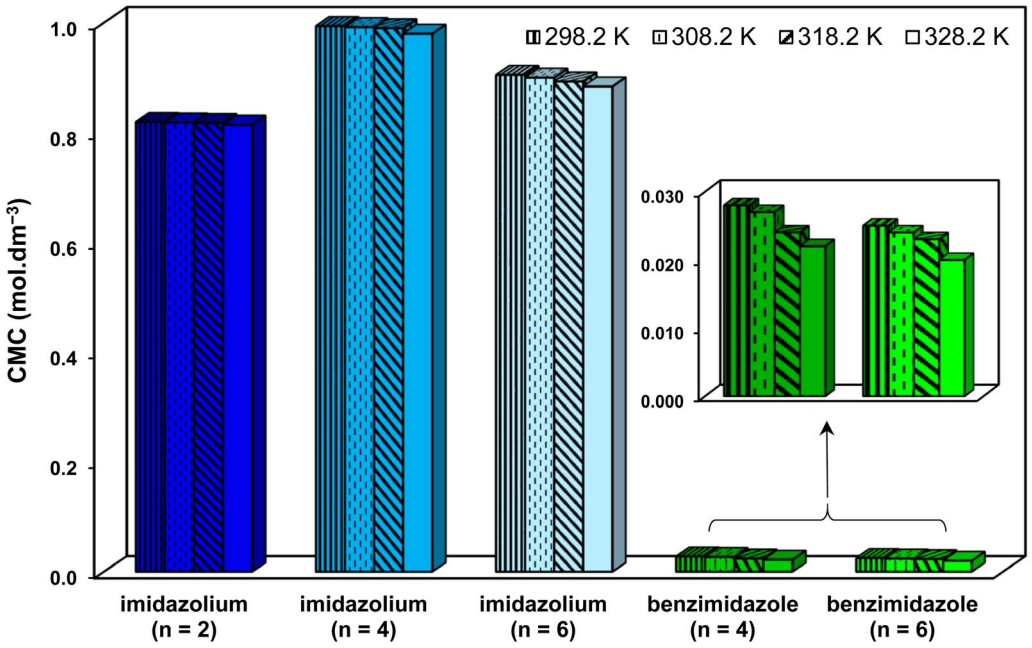

Fig. 10 Comparing CMC values of the benzimidazolium and the imidazolium GSAILs for the crude oil–water system at different temperatures.

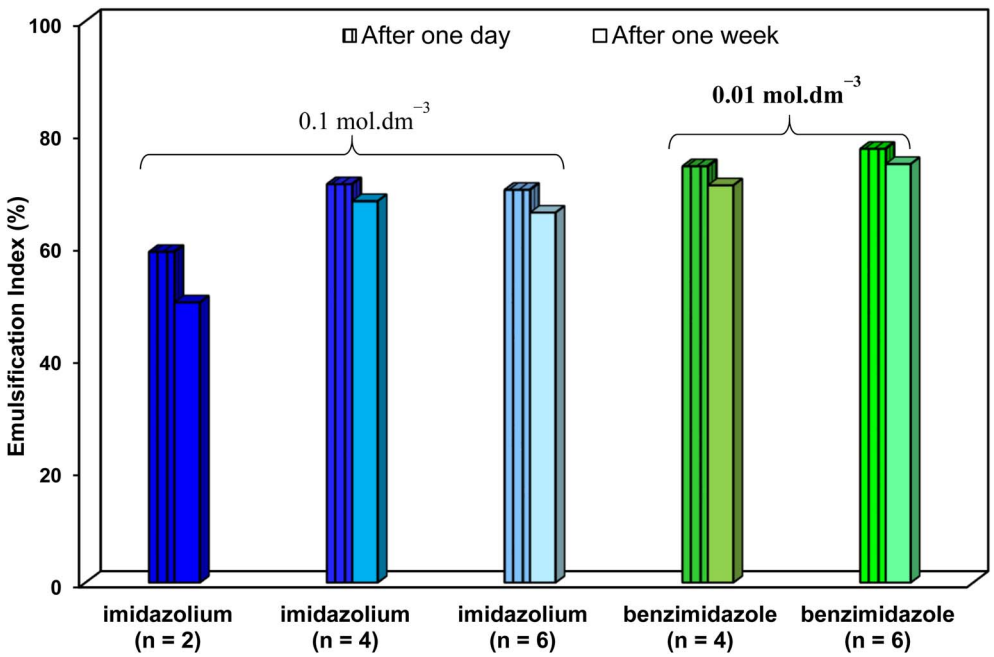

Fig. 11 Emulsification indices with 0.01 mol dm^{-3} of the benzimidazolium GSAILs and 0.1 mol dm^{-3} of the imidazolium GSAILs after one day and one week, all at 298.2 K.

aforementioned, greater hydrophobicity and lesser electrostatic repulsion increases the tendency of molecules to aggregate. This also confirms the higher absolute values of the free energy of micellization, ΔG°_{mic}, for the benzimidazolium GSAILs (see data in Tables 6 and 7). The benzimidazolium GSAILs also exhibit greater emulsifying capability. Fig. 11 shows that the emulsification indices are rather at the same levels whereas 0.01 and 0.1 mol dm^{-3} (corresponding to intermediate IFTs) concentrations have been corresponding to the benzimidazolium and the imidazolium GSAILs, respectively.

6. Conclusions

This contribution explores the effectiveness of the nanostructure benzimidazolium GSAILs in reducing the IFT and CMC as well as changing wettability and providing stable

emulsions of the crude oil–water system. The product synthesis was performed for the first time and the correctness was proved by various analysis methods.

Thanks to their unique structure, the products could highly decrease the crude oil–water IFT and the longer GSAIL spacer (six carbons chain) exhibited better performance due to greater hydrophobicity. Increasing temperature highly improved the performance of GSAILs. The well-known Frumkin adsorption isotherm was able to reproduce the experimental data and to determine the related factors and the thermodynamic parameters with reasonable variations *versus* temperature.

The surface wettability was obviously transferred from oil-wet to water-wet with either of the benzimidazolium GSAILs, as a consequence of reducing the adhesion of the crude oil to the solid surface. Further, emulsification study revealed that the GSAILs could provide very stable dispersions.

Compared to homologous imidazolium GSAILs, the greater effect of the benzimidazolium GSAILs in reducing IFT and CMC as well as increasing emulsification efficiency, at low concentrations was obvious. These can be attributed to the stronger hydrophobicity of the benzimidazole aromatic rings and better compensating the electrostatic repulsion between head groups, allowing easier adsorption as well as bulk aggregation at low concentrations.

The results totally showed that the novel nanostructure benzimidazolium GSAILs is a favorable alternative to conventional surfactants in enhanced oil recovery; though, applications at field should be sufficiently explored to find operational issues.

Author contributions

The manuscript was written through the contributions of all authors. All authors have given approval to the final version of the manuscript.

Conflicts of interest

The authors declare no competing financial interest.

Acknowledgements

The authors would like to acknowledge the Bu-Ali Sina University and also the Iran National Science Foundation: INSF, for their financial supports under Grant # 99031559.

References

1 E. Tamayo-Mas, H. Mustapha and R. Dimitrakopoulos, *J. Pet. Sci. Eng.*, 2016, **146**, 222–240.
2 P. Painter, P. Williams and A. Lupinsky, *Energy Fuels*, 2010, **24**, 5081–5088.
3 M. Kharazi, J. Saien and S. Asadabadi, *Top. Curr. Chem.*, 2022, **380**, 1–44.
4 J. Saien, M. Kharazi, V. Pino and I. Pacheco-Fernández, *Sep. Purif. Rev.*, 2022, 1–29.
5 Y. Takahashi, N. Koizumi and Y. Kondo, *Langmuir*, 2016, **32**, 683–688.
6 H. Zhou, Y. Zhu, T. Peng, Y. Song, J. An, X. Leng, Z. Yi, Y. Sun and H. Jia, *J. Mol. Liq.*, 2016, **223**, 516–520.
7 A. P. de los Ríos, A. Irabien, F. Hollmann and F. J. H. Fernández, *J. Chem.*, 2013, **2013**, 1–3.
8 A. Dharaskar Swapnil, *Res. J. Chem. Sci.*, 2012, **2231**, 80–85.
9 A. O. Diallo, C. Len, A. B. Morgan and G. Marlair, *Sep. Purif. Technol.*, 2012, **97**, 228–234.
10 A. Mero, A. Mezzetta, J. Nowicki, J. Łuczak and L. Guazzelli, *J. Mol. Liq.*, 2021, **334**, 115988.
11 I. Rodríguez-Palmeiro, I. Rodríguez-Escontrela, O. Rodríguez, A. Arce and A. Soto, *RSC Adv.*, 2015, **5**, 37392–37398.
12 E. Joonaki, H. R. E. Gahrooei and S. Ghanaatian, *J. Unconv. Oil Gas Resour.*, 2016, **15**, 11–21.
13 A. Ezzat, O. Ayman, M. Atta and H. A. Al-Lohedan, *Fuel*, 2021, **304**, 121436.
14 M. Kharazi and J. Saien, *J. Pet. Sci. Eng.*, 2022, **219**, 111090.
15 A. H. Ab Rahim, N. Abd Ghani, N. Hasanudin, N. M. Yunus and N. S. Azman, *Mater*, 2022, **15**, 1247.
16 A. Dhar, N. S. Kumar, M. Asif and R. L. Vekariya, *New J. Chem.*, 2018, **42**, 6990–6996.
17 W. Zhang, G. Huang, J. Wei, H. Li, R. Zheng and Y. Zhou, *J. Hazard. Mater.*, 2012, **235–236**, 128–137.
18 N. N. Al-Mohammed, Y. Alias and Z. Abdullah, *RSC Adv.*, 2015, **5**, 92602–92617.
19 C. Chen, S. Wang, M. J. Kadhum, J. H. Harwell and B. J. Shiau, *Fuel*, 2018, **222**, 561–568.
20 M. Kharazi, J. Saien, M. Yarie and M. A. Zolfigol, *Pet. Res.*, 2021, **117**, 113–123.
21 M. Kharazi and J. Saien, *ACS Omega*, 2022, **7**, 40042–40053.
22 J. Saien, M. Kharazi, M. Yarie and M. A. Zolfigol, *Ind. Eng. Chem. Res.*, 2019, **58**, 3583–3594.
23 S. Steudte, S. Bemowsky, M. Mahrova, U. Bottin-Weber, E. Tojo-Suarez, P. Stepnowski and S. Stolte, *RSC Adv.*, 2014, **4**, 5198–5205.
24 I. V. Kapitanov, A. Jordan, Y. Karpichev, M. Spulak, L. Perez, A. Kellett, K. Kümmerer and N. Gathergood, *Green Chem.*, 2019, **21**, 1777–1794.
25 M. T. Garcia, I. Ribosa, L. Perez, A. Manresa and F. Comelles, *Langmuir*, 2013, **29**, 2536–2545.
26 U. F. Haziz, R. A. Haque, A. Amirul, O. N. Aidda and M. R. Razali, *J. Organomet. Chem.*, 2019, **899**, 120914.
27 H. J. Jiang, R. Atkin and G. G. Warr, *Curr. Opin. Green Sustain. Chem.*, 2018, **12**, 27–32.
28 J. Łuczak, M. Paszkiewicz, A. Krukowska, A. Malankowska and A. Zaleska-Medynska, *Adv. Colloid Interface Sci.*, 2016, **227**, 1–52.
29 A. O. Gbadamosi, R. Junin, M. A. Manan, N. Yekeen, A. Agi and J. O. Oseh, *J. Ind. Eng. Chem.*, 2018, **66**, 1–19.
30 R. Hayes, G. G. Warr and R. Atkin, *Chem. Rev.*, 2015, **115**, 6357–6426.
31 A. Mezzetta, L. Guglielmero, A. Mero, G. Tofani, F. D'Andrea, C. S. Pomelli and L. Guazzelli, *Molecules*, 2021, **26**, 4211.
32 M. Kharazi, J. Saien, M. Yarie and M. A. Zolfigol, *J. Mol. Liq.*, 2019, **296**, 111748.

33 C. E. Stauffer, *J. Phys. Chem.*, 1965, **69**, 1933–1938.
34 J. Drelich, C. h. Fang and C. L. White, *Encycl. Surf. Colloid Sci.*, 2002, **3**, 3158–3163.
35 M. Lan, X. Wang, P. Chen and X. Zhao, *Case Stud. Therm. Eng.*, 2016, **8**, 218–225.
36 J. Saien, M. Kharazi and S. Asadabadi, *Iran. J. Chem. Eng.*, 2015, **12**, 59–74.
37 H. Amani, *Pet. Sci. Technol.*, 2015, **33**, 510–519.
38 P. Pillai, A. Kumar and A. Mandal, *J. Ind. Eng. Chem.*, 2018, **63**, 262–274.
39 L. Zhang, Y. Geng, W. Duan, D. Wang, M. Fu and X. Wang, *J. Sep. Sci.*, 2009, **32**, 3550–3554.
40 M. J. Rosen, H. Wang, P. Shen and Y. Zhu, *Langmuir*, 2005, **21**, 3749–3756.
41 S. K. Nandwani, N. I. Malek, M. Chakraborty and S. Gupta, *Energy Fuels*, 2020, **34**, 6544–6557.
42 L. He, F. Lin, X. Li, H. Sui and Z. Xu, *Chem. Soc. Rev.*, 2015, **44**, 5446–5494.
43 Z. H. Guang, D. A. Caili and Y. O. Qing, *Pet. Explor. Dev.*, 2018, **45**, 481–490.
44 Z. Yazhou, W. Demin, W. Zhipeng and C. Rui, *Pet. Explor. Dev.*, 2017, **44**, 111–118.
45 A. Mandal, A. Samanta, A. Bera and K. Ojha, *Ind. Eng. Chem. Res.*, 2010, **49**, 12756–12761.
46 T. Hussein Ali, R. Syahila Duali Hussen, T. Heidelberg and H. Anua Bin Tajuddin, *ChemistrySelect*, 2020, **5**, 6856–6860.
47 A. Bera and H. Belhaj, *J. Mol. Liq.*, 2016, **224**, 177–188.
48 I. Rodríguez-Escontrela, I. Rodríguez-Palmeiro, O. Rodríguez, A. Arce and A. Soto, *Fluid Phase Equilib.*, 2016, **417**, 87–95.
49 B. Gao and M. M. Sharma, *J. Colloid Interface Sci.*, 2013, **404**, 80–84.
50 K. S. Birdi, *Surface and Colloid Chemistry: Principles and Applications*, CRC press, 2009.
51 C. Stubenrauch, V. B. Fainerman, E. V. Aksenenko and R. Miller, *J. Phys. Chem. B*, 2005, **109**, 1505–1509.
52 D. Möbius, R. Miller and V. B. Fainerman, *Surfactants: Chemistry, Interfacial Properties, Applications*, Elsevier, 2001.
53 G. Liu, D. Gu, H. Liu, W. Ding, H. Luan and Y. Lou, *J. Colloid Interface Sci.*, 2012, **375**, 148–153.
54 K. Motomura, S. I. Iwanaga, M. Yamanaka, M. Aratono and R. Matuura, *J. Colloid Interface Sci.*, 1982, **86**, 151–157.
55 S. Asadabadi, J. Saien and V. Khakizadeh, *J. Chem. Thermodyn.*, 2013, **62**, 92–97.
56 H. Matsubara, A. Onohara, Y. Imai, K. Shimamoto, T. Takiue and M. Aratono, *Colloids Surf., A*, 2010, **370**, 113–119.